Particle Accelerators, 1992, Vol. 39, pp. 15–32
Reprints available directly from the publisher
Photocopying permitted by license only

© 1992 Gordon and Breach Science Publishers, S.A.
Printed in the United Kingdom

DISSIPATIVE BEAM TRAPPING IN A MODIFIED BETATRON WITH STRONG FOCUSING

Y. SEO† and P. SPRANGLE

Plasma Physics Division, Naval Research Laboratory, Washington D.C. 20375.

(Received 11 October 1990; in final form 19 September 1991)

Beam trapping schemes in a modified betatron with strong focusing fields, utilizing dissipative forces, are investigated. Sources that are considered for the dissipative forces are the image field and the wakefield associated with a resistive wall, as well as the electrostatic field due to background ions. It is concluded that, with an ultra high electron beam current (greater than 1 kA), these forces can provide a fast enough inward drift to the center of the minor axis of the chamber to cause beam trapping.

1 INTRODUCTION

Over the last several decades, physicists have developed highly sophisticated high-energy accelerator technology to probe the structure of matter on a subnuclear scale. These accelerators have operated at relatively low currents, mainly to avoid the complications due to the self-fields of the accelerating charged particles. It is expected, however, that electron beams having both high energy and current could have many applications in a wide variety of areas, ranging from national defense to x-ray radiology, food preservation and environmental protection.[1] Studies on ultrahigh-current electron accelerators are now being carried out by several research groups[2]. These studies include the modified betatron research at the Naval Research Laboratory (NRL).

Among the various accelerating schemes that have the potential to produce ultrahigh-power electron beams, cyclic induction accelerators[3], such as conventional and modified betatrons, have many advantageous features. Cyclic devices are inherently compact, and the acceleration is continuous. This is in contrast to linear devices, in which the acceleration is localized in the gaps. As a result, the peak power requirements of cyclic induction accelerators are much lower than those of linear induction accelerators.

The conventional betatron has a time-varying vertical magnetic field (betatron field) generating an inductive, toroidal accelerating electric field. The orbital radius of the electron beam remains constant during acceleration if the flux rule is satisfied—that is, if the rate of change of the average magnetic field within the beam orbit is twice the rate of change of the local field at the position of the beam. The

† Permanent address: FM Technologies, Inc., Fairfax, VA 22032.
Present address: Dept. of Physics, Kwang-Woon Univ., 447-1 Wallgye-Dong, Nowon-Gu, Seoul, Korea.

electron beam current in a conventional betatron is limited by the space-charge orbital instability: a tendency for the beam to expand/defocus due to the space charge. Limitations from the various collective beam instabilities, such as the negative mass instability, are also stringent. The negative mass instability causes electrons to be bunched along the direction of the beam propagation, inducing an expansion of the minor radius of the beam.

The modified betatron has a guiding toroidal magnetic field in addition to the betatron field.[4] In contrast to the betatron field, which affects mainly the major radius of the electron ring, the toroidal magnetic field affects primarily the beam's minor radius. The stability of the beam, in comparison to that of the conventional betatron, is greatly improved by the strong toroidal field. For example, the space-charge orbital instability is greatly reduced so that the space charge limiting current is enhanced by a factor of $B_0^2/2B_\perp^2$, where $B_0(B_\perp)$ is the toroidal (betatron) magnetic field. Hence, by having $B_0 \gg B_\perp$, the current allowed in a modified betatron can be much higher than in conventional betatrons. The modified betatron also tolerates a large beam emittance. The toroidal field, however, does not cure some of the problems associated with the conventional betatrons, namely, the orbit's sensitivity to the energy mismatch and the orbit disruption by the self-magnetic-field diffusion. Moreover, the beam centroid is unstable due to the drag instability.[5]

To overcome these additional problems the NRL modified betatron has been equipped with an additional focusing field, a rotating quadrupole (stellarator) field (Figure 1). The energy sensitivity is greatly reduced by this field.[6] The price one pays is increased complexity in coil design and beam injection. As far as the beam injection is concerned, however, it has been noticed that the drag instability causes a negative growth rate in the presence of the stellarator field, so the beam centroid is trapped to the center of the vacuum chamber. Sprangle and Kapetanakos[7] have considered the trapping behavior due to an induced image field on the surrounding resistive wall as a source of the drag force. This paper is an extension to that report, considering various other possible sources for the drag force.

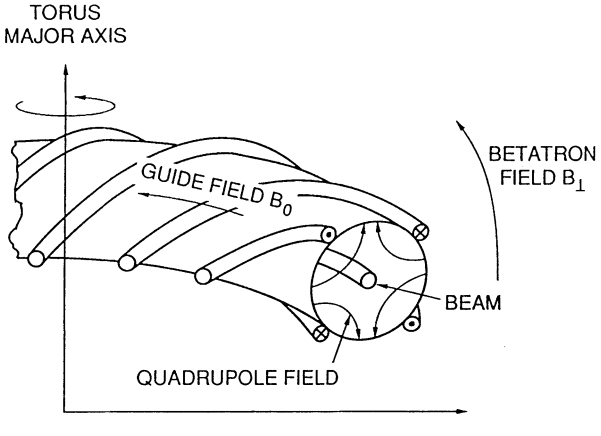

FIGURE 1 Schematic configuration of the modified betatron with strong focusing stellarator coils.

Section 2 gives a brief review of the physical mechanism of the dissipative beam trapping in a modified betatron with stellarator field. For more details, Reference 7 is recommended. Section 3 investigates the effect of wakefields due to a resistive wall, and Section 4 considers the effect of background ion production. The relevance of these schemes to the beam trapping observed in the NRL modified betatron is estimated in Section 5. It is concluded that both of the trapping schemes have difficulties on explaining the experimental observations. Concluding remarks are made in Section 6.

2 TRAPPING BY DRAG FORCES

For simplicity we neglect the toroidal effects and work in a straight cylindrical geometry. It turns out, however, that the periodicity of a toroidal system becomes important in considering the effect of the wakefields, and we will put in the periodicity by hand when necessary. The external fields we consider are a constant guiding field $-B_0\hat{z}$, where $-\hat{z}$ is a unit vector in the direction of beam propagation, and a linearized rotating quadrupole field

$$b_x = b_0 k_w (y \cos k_w z - x \sin k_w z),$$

$$b_y = b_0 k_w (x \cos k_w z + y \sin k_w z),$$

where x, y, and z form a right handed Cartesian coordinates, $2\pi/k_w$ is the period of the rotating field, and $b_0 k_w$ is the field gradient. We also include the fields from the induced charges and currents on the wall of the vacuum chamber,

$$\mathbf{E}_{\text{ind}} = \frac{-2m_0c^2}{e}\frac{\nu}{a^2}(x(t)\hat{x} + y(t)\hat{y}), \tag{1}$$

$$\mathbf{B}_{\text{ind}} = \frac{2m_0c^2}{e}\frac{\nu}{a^2}\beta_0(y(t)\hat{x} - x(t)\hat{y}), \tag{2}$$

where m_0 and $-e$ are the electron rest mass and charge, respectively, c is the speed of light, ν is Budker's parameter, $\beta_0 c$ is the axial beam velocity, and a is the radius of the vacuum chamber. Here we are assuming that the location of electron beam is close to the center of the chamber, that the beam radius r_b is much less than the wall radius a, and that the wall has infinite conductivity. Notice that the forces due to the induced electric and magnetic fields are related by $\mathbf{F}_B = -\beta_0^2\mathbf{F}_E$, so the magnetic force partially cancels the electric force. Under influence of these fields, the equation of motion for the beam centroid is

$$\ddot{u}(t) + i\Omega_0\dot{u}(t) - \omega_s^2 u(t) - \omega_0\omega_w e^{i\omega_w t}u^*(t) = 0, \tag{3}$$

where $u(t) = x(t) + iy(t)$, $\Omega_0 = eB_0/\gamma_0 m_0 c$, $\omega_0 = eb_0/\gamma_0 m_0 c$, $\omega_w = k_w\beta_0 c$, $\omega_s^2 = 2c^2\nu/(\gamma_0^3 a^2)$, and $\gamma_0 = (1 - \beta_0^2)^{-1/2}$. Here, we have replaced $k_w z$ with $-\omega_w t$, assuming that the axial beam velocity is a constant. Assuming that Ω_0 is much greater than all other frequencies, we decompose the guiding center motion into a slow average drift

and an oscillation around the drift center, i.e., $u = u_c + \delta u$. Here δu is provided by the oscillation of the quadrupole field, which we can write $\delta u = \delta u_+ \exp(i\omega_w t) + \delta u_- \exp(-i\omega_w t)$. Substituting these for $u(t)$ and time-averaging over $2\pi/\omega_w$, we get the drift center equation,

$$\dot{u}_c(t) = i\omega_B u_c(t), \tag{4}$$

with

$$\omega_B = \frac{1}{\Omega_0}\left[\frac{\omega_0^2\omega_w^2}{\omega_w(\Omega_0 + \omega_w) + \omega_s^2} - \omega_s^2\right] \approx \left(\frac{\omega_0}{\Omega_0}\right)^2 \omega_w - \frac{\omega_s^2}{\Omega_0}, \tag{5}$$

and an oscillatory motion

$$\delta u_- = 0,$$

$$\delta u_+ = -\frac{\omega_0\omega_w}{\omega_w(\Omega_0 + \omega_w) + \omega_s^2}\, u_c^* \approx \left(\frac{\omega_o}{\Omega_0}\right) u_c^*,$$

which is small when $\omega_0 \ll \Omega_0$. Equation (4) tells us that the drift center rotates around the chamber axis with a frequency ω_B. When $\omega_0 = 0$, i.e., when there is no strong focusing, the drift motion corresponds to an $\mathbf{F} \times \mathbf{B}$ drift, with a $\mathbf{F}$ from an attractive force on the beam by the image charges, partially cancelled by a repulsive force by the image current. Hence, $\mathbf{F}$ is directed radially outward to the wall, and the beam rotates clockwise assuming $\Omega_0 > 0$. On the other hand, when there is a focusing field with a polarity such that ω_w is positive, ω_B changes its sign when the field strength (ω_0) is sufficiently large. The beam rotates counterclockwise in this case, and it can be said that the effective force $\mathbf{F}$ for the $\mathbf{F} \times \mathbf{B}$ drift is directed inward to the center of the chamber. This change of directionality is important once we impose a small tangential force $\mathbf{F}_d$ (drag force) in addition. The drag forces are dissipative in nature, and always oppose the beam motion. Hence, $\mathbf{F}_d \times \mathbf{B}$ results in a radially outward (inward) drift when $\mathbf{F}$ is directed outward (inward). In other words, the drag force causes an inward drift (beam trapping) when there is a strong focusing field which reverses the drift direction (Figure 2).

The inward drift (trapping) of the beam centroid can be used for beam injection into the accelerator when the following requirements are satisfied: (i) ω_B is sufficiently large so that the beam rotates far enough not to hit the injector when it returns from a round trip around the torus; and (ii) the inward drift is fast enough to avoid hitting the injector by the time the beam completes one bounce oscillation, i.e., at $t = 2\pi/\omega_B$. From the first requirement, assuming that the beam radius and the injector size are on the order of a centimeter, and that the major radius of the accelerator is on the order of a meter, we can expect that ω_B must be of order 10^7sec^{-1} or greater. This sets the upper limit of the bounce time ($2\pi/\omega_B$) at around 1 μs. The second requirement tells us that the decay time must be also less than a few microseconds. Table 1 shows various physical parameters relevant to the NRL modified betatron with strong focusing.

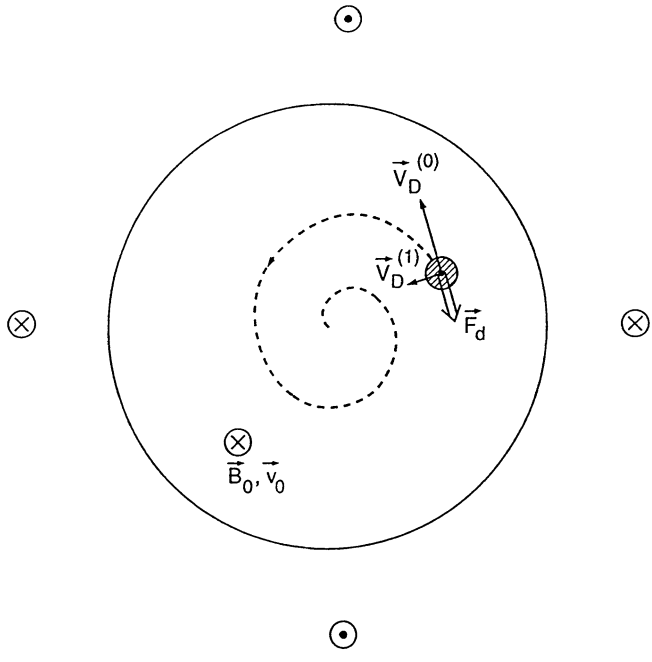

FIGURE 2 A schematic view of the electron beam being trapped to the center of the minor cross section due to a drag force (dotted line). $\mathbf{v}_D^{(0)}$ is the zeroth order average drift velocity. $v_D^{(1)} \sim -\mathbf{F}_d \times \mathbf{B}_0$ is the inward drift velocity caused by the drag force $\mathbf{F}_d$.

3 RESISTIVE WALL EFFECTS

In this section we consider the effects of a resistive wall as a source of dissipation. When the wall has finite conductivity, the magnetic field of the beam penetrates into the wall with a finite diffusion time. This diffusion time also characterizes the decay time of the induced current on the wall, so a long-tailed residual current changes the magnetic field configuration around the electron beam. Generally, the induced magnetic field can be expressed in the following form, assuming that the beam is

Table 1 Design Parameters of NRL Modified Betatron

Torus major radius [m]	1
Torus minor radius, a [cm]	15
Guiding magnetic field, B_0 [kG]	2–3
Focusing field gradient, $b_0 k_w$ [G/cm]	15–20
Focusing field wavenumber, k_w [cm^{-1}]	0.06
Electron beam radius, r_b [cm]	1
Electron injection energy, γ_0	2
Injection position, $u(0)$ [cm]	8
Wall conductivity, σ [sec^{-1}]	3×10^{14}
Wall thickness [cm]	0.32

located near the center:

$$\mathbf{B}_{\text{ind}} = \frac{2m_0c^2}{e}\frac{v}{a^2}\beta_0\int_0^t d\tau\ G(t-\tau)(y(\tau)\hat{x} - x(\tau)\hat{y}). \tag{6}$$

Here $G(t)$ is the Green's function for the magnetic field diffusion. Equation (6) reduces to Equation (2) when $G(t) = \delta(t)$, the Dirac delta function.

3.1 Self-consistent solution in an infinitely long cylinder

Let us assume that an infinitely long line of beam current is turned on instantaneously at a time $t = 0$, i.e., $I(t) = I_0\theta(t)$, where $\theta(t) = 1$ for $t > 0$, 0 for $t < 0$. If we further assume that (skin depth) < (wall thickness) $\ll a$, then $G(t)$ is given by:[5]

$$G(t) = \delta(t) - \frac{c}{\pi a}(\sigma t)^{-1/2}, \tag{7}$$

where σ is the conductivity of the wall. With the fields of (6) and (7) we find that the average drift motion of the beam centroid satisfies

$$\dot{u}_c(t) - i\omega_B u_c(t) = i\frac{\omega_s^2}{\Omega_0}\gamma_0^2\beta_0^2\int_0^t d\tau\ \delta G(t-\tau)u_c(\tau). \tag{8}$$

Here $\delta G(t) = G(t) - \delta(t)$, and the convolution integral has been time averaged over $2\pi/\omega_w$. Equation (8) is solved by the Laplace transform. The solution can be written as

$$u_c(t) = L^{-1}\left[\frac{u_c(0)}{s - i\omega_B - i\omega_A\delta\tilde{G}(s)}\right], \tag{9}$$

where $\delta\tilde{G}(s) = L[\delta G(t)] = -c/(a\sqrt{\pi\sigma s})$, $\omega_A = \omega_s^2\,\gamma_0^2\beta_0^2/\Omega_0$, and $L(L^{-1})$ denotes the (inverse) Laplace transform. The Laplace transform of (9) has a pole at

$$s = s_0 \simeq i[\omega_B - \omega_A(\delta_B/a)] - \omega_A(\delta_B/a). \tag{10}$$

Here, $\delta_B = c/\sqrt{2\pi\sigma\omega_B}$ is the skin depth corresponding to the bounce frequency ω_B, and $\omega_A\delta_B/a \ll \omega_B$ is assumed. This pole indicates the time-asymptotic decay rate of the drift center radius to be $\Gamma \sim -\text{Re}(s_0) = \omega_A(\delta_B/a)$. Noticing that (9) has a branch point $s = 0$, we choose the contour for inverse transform as in Figure 3. Then, we obtain

$$u_c(t) = u_c(0)\left[\frac{e^{s_0t}}{1 - \dfrac{i\alpha}{2s_0^{3/2}}} + \frac{\alpha}{i\pi}\int_0^\infty ds\,\frac{e^{-st}\sqrt{s}}{s(s+i\omega_B)^2 - \alpha^2}\right], \tag{11}$$

where $\alpha = \omega_A c/(a\sqrt{\pi\sigma})$. The second term in the form of integral is a contribution of the branch cut.

Figure 4 shows a plot of the solution of (11), $R(t) = |u_c(t)|$, when $\alpha = 0.2\omega_B^{3/2}$. The time scale is ω_B^{-1}. Taking $\omega_B \sim 10^7\ \text{sec}^{-1}$ and other parameters as in Table 1, the plotted solution corresponds to an electron beam current of ~ 5 kA. The dotted line

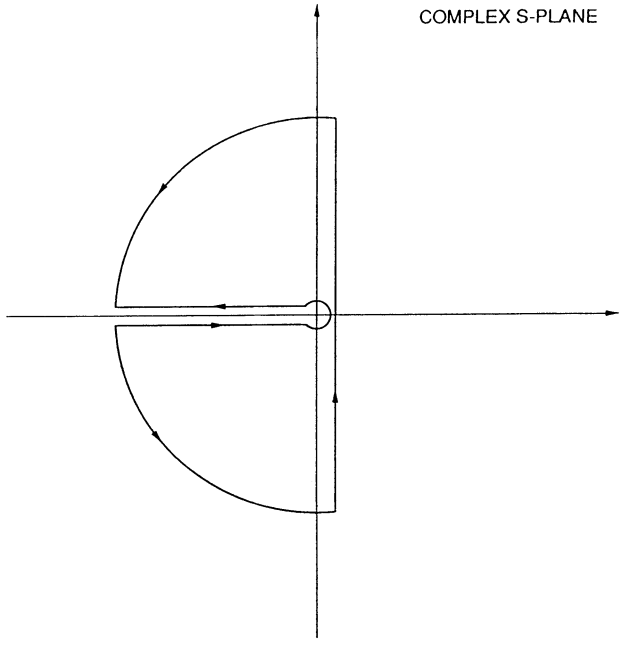

FIGURE 3 Contour for the inverse Laplace transform.

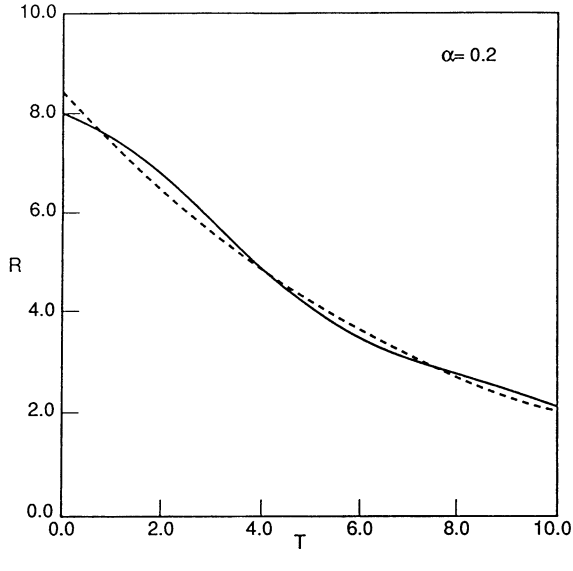

FIGURE 4 Plot of the solution (11) for $\alpha = 0.2\omega_B^{3/2}$; $R(t) = |u_c(t)|$. Dotted line follows the value of the first term. Time T is in unit of ω_B^{-1}.

in the figure plots the value of the first term alone, which is an exponential decay. The actual solution (solid line) wiggles about the exponential function. This wiggling behavior is due to the wakefield as will be shown later. In a straight cylindrical geometry, the wakefield contribution to the decay rate is small as we see in the figure. In a toroidal geometry, however, it will be shown that the contribution is not minor.

3.2 *Physical interpretation*

We now investigate the physical meanings of the two terms in the solution to Equation (11)—and consider how that solution should be modified when the electron beam circulates in a torus rather than propagates in a straight cylinder. To do that, we find it more appropriate to consider the resistive wall effect as a perturbation to the zero-order motion in a perfectly conducting wall. In this regard, we first assume that the beam is executing its zero-order motion, and then estimate what the induced field is under that beam motion and how this field changes the zero-order motion.

Let us begin with expressing the induced magnetic field (Eq. (6)) in cylindrical polar coordinates (r, θ);

$$B_{\text{ind},r}(r, \theta, t) \simeq \frac{iI_0}{ca^2} e^{i\theta} \int_0^t G(t-\tau)u_c^*(\tau)d\tau + c.c., \tag{12}$$

where $B_{\text{ind},r}$ is the radial component, $u_c^*(\tau) = r_0 \exp(-i\omega_B\tau)$ for the zeroth order motion, r_0 is the radius of the beam position, $G(t) = \delta(t) - (c/\pi a)(\sigma t)^{-1/2}$, I_0 is the beam current, and *c.c.* stands for the complex conjugate. We keep track of the radial component of the induced field because the field direction gives rise to a radial drift. The poloidal component results only in a minor modification of the bounce frequency. With the contour in Figure 3, the convolution integral in (12) leads to

$$r_0 \int_0^t d\tau\, Ge^{-i\omega_B\tau} = r_0 e^{i\omega_B t} - \frac{2r_0}{a} \frac{c}{\sqrt{4\pi\sigma}} \left[\frac{e^{i\omega_B t}}{\sqrt{-i\omega_B}} - \frac{\sqrt{t}}{\pi} \int_0^\infty ds \frac{e^{-s}}{\sqrt{s(s - i\omega_B t)}} \right] \tag{13}$$

The first two terms in (13) have the same time dependence. Being combined, they give the induced image field

$$B_{\text{image},r} = \frac{2I_0 r_0}{ca^2} \left[\left(1 + \frac{\delta_B}{a}\right)^2 + \left(\frac{\delta_B}{a}\right)^2 \right]^{1/2} \sin(\theta - \omega_B t - \psi), \tag{14}$$

where $\tan\psi = \delta_B/(a + \delta_B)$. We observe that the image field has been rotated by an angle $\psi \approx \delta_B/a$. Physically, we can say that the effective location of the image current has been shifted; θ(Image current) $\simeq \theta$(beam) $+ \psi$. It seems that the shifting term, which is the first term in the bracket of (13), diverges when $\omega_B \to 0$. Actually, this term is large when ω_B is small since the magnetic field penetrates deeply into the wall. However, as soon as the skin depth becomes greater than the wall thickness, the expression for δG, Equation (7), needs modification, and we can indeed show that the term disappears when $\omega_B = 0$.

Time dependence of the last term in (13) suggests that the term is related more to

the initial boundary condition than to the subsequent beam dynamics. The term is transient; it decays as $1/\sqrt{t}$ at large $\omega_B t$. When $\omega_B t \ll 1$, however, the term gives a magnetic field growing as $\sqrt{t}$:

$$B^{(1)}_{\text{wake},r} \approx \frac{2I_0 r_0}{ca^2} \sqrt{\frac{8}{\pi}} \frac{\delta_B}{a} (\omega_B t)^{1/2} \sin\theta. \tag{15}$$

We will identify (15), or equivalently the last term of (13), as a wakefield. Adding (14) and (15), the total induced field at $\omega_B t \ll 1$ is

$$\begin{aligned} B_{\text{ind},r}(\theta, t) &= B_{\text{image},r} + B^{(1)}_{\text{wake},r} \\ &\approx \frac{2I_0 r_0}{ca^2} \left\{ \sin(\theta - \omega_B t) - \frac{\delta_B}{a} \left[\cos(\theta - \omega_b t) + \left(\frac{8}{\pi} \omega_B t \right)^{1/2} \sin\theta \right] \right\}, \end{aligned} \tag{16}$$

where we have kept only the terms up to the linear ones in δ_B/a. An interesting aspect to notice is that the wakefield, which depends on $\sin\theta$, is zero at the position of the beam ($\theta \approx 0$ since we are at $\omega_B t \ll 1$). Hence, without the drift motion the beam does not feel its own wakefield (as far as B_r is concerned). As the drift proceeds, the beam begins to feel the wakefield, which, however, has largely decayed. This is why the wakefield makes only a minor contribution to the solution (11), as we see from Figure 4.

Chao[8] gives an illuminating wakefield solution of a cylindrical resistive wall, assuming that the charges propagate at the speed of light. He shows that the asymptotic[9] wakefield made by a ring-shaped charge distribution with a density $\rho = (M_1/\pi b^2)\delta(z - ct)\delta(r - a)\cos\theta$, where $M_1(b)$ is the ring dipole moment (radius), is given by

$$B^{(2)}_{\text{wake},r} = -\sqrt{\frac{c}{\sigma}} \frac{2M_1}{\pi a^3} \frac{\sin\theta}{|z - ct|^{1/2}}, \qquad z - ct < 0 \tag{17}$$

(Here, we have neglected the field that dies away as $|z - ct|^{-5/2}$.) Integrating (17) with respect to z, we can obtain the wakefield made by a straight line of charges (beam) placed off-axis by a small distance so that its dipole moment is M_1. Taking the integration range to be finite, say from $z = 0$ to $z = l$, this is more realistic for describing a beam coming out of an injector in an accelerator than for a beam instantaneously turned on everywhere. Especially since we are interested in a transient phenomenon, different boundary conditions may imply different solutions. The solution (17), however, is valid only in the limit that the beam propagation velocity is equal to the speed of light. Advantages in getting the solution with this limit are apparent. Since the self-field of the ring is Lorentz-contracted into a longitudinally infinitesimal volume, a direct influence on the wall is made only where the ring is. Hence, there is no confusion with causality. The wakefield is simply the field made behind the ring.

Let us now compare the two solutions: (15) in the limit of $\omega_B \to 0$ and the integrated form of (17). We first notice that both fields grow as $t^{1/2}$ and $|z - ct|^{1/2}$, which are identical behaviors for their boundary conditions. In fact, the two fields are identical

if we identify M_1 for (17) with $I_0 r_0/c$. Now, their identity suggests two important conclusions. First, (15) is indeed the wakefield made by an infinite line of current that is instantaneously turned on at $t = 0$. Second, since we did not assume the beam velocity to be the speed of light in order to get (15), the wakefield solution (17), *in its integrated form*, is still valid at a propagation velocity less than the speed of light. We can given an intuitive explanation for this. Let us imagine a point charge propagating with a speed of light. Because of the Lorentz contraction, its electric and magnetic self-fields are confined in a transverse disc of an infinitesimal thickness. Now, as we reduce the velocity, the disc expands such that the subtended angle of field confinement is of order $1/\gamma$, and the field is not transverse everywhere any more. However, if we imagine the (integrated) field as being created by a line of charges instead of a point source, the longitudinal components cancel out and we get the same self-field structure whether the charges propagate at the speed of light or not. In other words, both systems have identical wakefields because their self-fields do not have any fringe fields that come from edges. Since the same self-field penetrates into the wall, we must have the same induced field, including the wakefield.

A little comment can be made for the temporal behavior of the last term of (13). When $\omega_B t \ll 1$ and therefore the beam bounce motion can be neglected, the wakefields pile up to give a $\sqrt{t}$ growth. If the current were sustained at its initial location the field would grow indefinitely. The bounce motion of the beam, however, stops the growth by canceling the former wakefield with the latter with a rotated polarity. Eventually, the wakefield decays as $1/\sqrt{t}$ after a few bounce time through this cancellation.

3.3 *Wakefields in a toroidal accelerator*

We now consider the effects of the wakefield in a toroidal accelerator. We are considering only the effects of periodic characteristics of the torus, not the effect of curvature. Assuming that the torus minor radius is much less than the major radius, we neglect the self-field fringes at the beam front and tail, and use the wakefield of Section 3.2. Let us imagine a beam front coming out of the injector at a time $t = 0$. Let the injector be located at $z = 0$, and the major radius of the torus be $l/2\pi$. The beam front returns to the $z = 0$ minor cross section at a time $t_0 = l/\beta_0 c$. For simplicity let us assume that the beam pulse length is equal to t_0, so that at time $t > t_0$ the electron beam forms a single ring around the torus. During the one round trip, the beam front rotates by an angle $\theta_0 = \omega_B t_0$ in the minor cross section. Hence, the electron ring is not closed. Imagine that we are sitting on an arbitrary minor cross section. We would observe all the beam particles, from the front to the tail, hitting the cross section at the same angular position $\theta = \theta(0) + \omega_B t_1 = \theta_1$, where t_1 is the transit time from the injector to the minor cross section we are sitting on. The beam does not temporally rotate at the given cross section during the one-round-trip time. Consequently, the local wakefield made by each portion of the beam would pile up during a time interval t_0, giving a wakefield

$$B_{\text{wake},r}(z = z_1) = -\frac{2I_0 r_0}{ca^2}\frac{\delta_B}{a}\sqrt{\frac{8}{\pi}}\,[\omega_B(t - t_1)]^{1/2}\sin(\theta - \theta_1),\ t_1 \le t < t_0 + t_1. \quad (18)$$

Without loss of generality, we confine our sight to the $z = 0$ minor cross section, i.e. $t_1 = 0$, and $\theta_1 = \theta(0) \equiv 0$. We cut the time at each integer multiple of t_0 and find the wakefield *at the position of the beam* in each interval:

i) $0 \leq t < t_0$: $B_{\text{wake},r} = 0$ since beam is at $\theta = 0$.

ii) $t_0 \leq t < 2t_0$: There are two contributions to the wakefield; a beam that had passed during $0 \leq t < t_0$ at an angle $\theta = 0$, and a beam that is currently passing at an angle $\theta = \theta_0$. The former gives

$$B_{\text{wake},r} \sim -\int_{t'=t-t_0}^{t'=t} \frac{dt'}{t'^{1/2}} = -2(\sqrt{t} - \sqrt{t-t_0}). \tag{19}$$

Hence, adding with the latter,

$$B_{\text{wake},r} \sim -\sqrt{t-t_0}\,\sin(\theta - \omega_B t_0) - (\sqrt{t} - \sqrt{t-t_0})\sin\theta.$$

At the position of the beam ($\theta = \omega_B t_0$)

$$B_{\text{wake},r} \sim -(\sqrt{t} - \sqrt{t-t_0})\sin\omega_B t_0.$$

iii) $(n-1)t_0 \leq t < nt_0$: At the beam position $\theta = (n-1)\omega_B t_0$,

$$B_{\text{wake},r} \sim -(\sqrt{t} - \sqrt{t-t_0})\sin[(n-1)\omega_B t_0] - (\sqrt{t-t_0} - \sqrt{t-2t_0})\sin[(n-2)\omega_b t_0]$$
$$-\cdots - (\sqrt{t-(n-2)t_0} - \sqrt{t-(n-1)t_0})\sin\omega_B t_0.$$

Note that the fields at $z \neq 0$ can be obtained just by adding a time lag t_1. Now we wish to estimate the wakefield at the beam front. The beam front passes the $z = 0$ cross section at times $t = nt_0$ ($n = 0, 1, \ldots$). Hence, the field at the $z = 0$ cross section is

$$\begin{aligned} &t = 0 \qquad B_{\text{wake},r} \sim 0 \\ &t = t_0 \qquad B_{\text{wake},r} \sim -\sqrt{t_0}\sin\omega_B t_0 \\ &t = 2t_0 \qquad B_{\text{wake},r} \sim -\sqrt{t_0}\sin\omega_B t_0 - \sqrt{t_0}(\sqrt{2} - \sqrt{1})\sin 2\omega_B t_0 \end{aligned} \tag{20}$$

At $z = z_1 \neq 0$ the field lags by the transit time t_1, which is exactly cancelled by the time lag before the beam front arrives at that cross section. Hence, the fields in (20) are the ones at the beam front in each time interval, $(n-1)t_0 \leq t < t < nt_0$ ($n = 1, 2, \ldots$). Taking $\omega_B t_0 = \pi/6$, for example, the wakefield (20) becomes maximum at the sixth turn, so the total decay (trapping) rate in that time interval is about 2.7 times greater than the one due to the image field shift alone (10). The average decay rate during the first bounce period (12 turns) is also enhanced by a factor of 2.3. These decay rates are not sensitive to the value of $\omega_B t_0$.

4 EFFECTS OF BACKGROUND IONS

When the electron beam is injected into the vacuum chamber, electrons will immediately encounter residual air molecules and will ionize them. In this section

we consider this electron-impact ionization as a possible source for the beam trapping. Let us assume that the created ions are so heavy that they do not see any external magnetic fields. As stated in Section 2, the time scale for the beam trapping is of order 1 μs or less. Comparing this to the cyclotron frequency of a nitrogen ion in a magnetic field of ~ 1 kG, $\Omega_c \sim 3.4 \times 10^5$ sec^{-1}, we find that the assumption is not stringent. Let us also assume that the thermal velocity of ions is negligible. The ion motion, then, can be described by the electrostatic interaction with the electron beam. The latter, however, drifts in the minor cross section with a bounce frequency ω_B. If this drift is fast enough that the drift velocity of the beam may provide ions with an effective kinetic energy (in the beam drift frame) comparable to the electrostatic potential energy, the ions can escape from the potential field left behind the drifting beam. Then the ion self-field, in turn, attracts the electron beam against its drift, acting as a drag force on the beam.

In order to describe the interaction between the ions and the electron beam in a way that is appropriate for a numerical approach, we model the ion distribution with discrete beamlets, each having an infinitesimal radius. For example, we can form an ion beamlet by collecting the ions produced in a time interval $(t - \delta t/2,\ t + \delta t/2)$, and place them at the location of the electron-beam center at time t. Here, the time interval δt is assumed to be much less than ω_B^{-1}. If the drift velocity of the electron beam is large enough, the exact initial location of the ion beamlet would not be important, since the ions would spend most of the time out of the electron beam. Let N_i be the ion line density of the ith ion beamlet. The probability for a neutral molecule to be ionized in a time interval δt_i can be expressed with $(\sigma_s n_e v_0)\delta t_i$, where σ_s is the ionization cross section, n_e is the beam electron density, and v_0 is the electron velocity. To get the line density N_i of ions we may multiply the total number of neutrals per unit length inside the electron beam, $\pi r_b^2 n_0$, where n_0 is the density of the neutrals. Hence,

$$N_i = \delta t_i \cdot (\sigma_s n_e v_0)(\pi r_b^2 n_0).$$

The ionization cross section depends on the energy of the impacting electrons; $\sigma_s \sim 10^{-17}$ cm^2 at 10 keV, and $\sim 10^{-18}$ cm^2 at 0.5 MeV ($\gamma_0 = 2$).[10]

Let us assume that the electron density inside the beam radius r_b is uniform. The electrostatic potential made by the electron beam is then parabolic inside the beam and logarithmic outside. With this potential the equation of motion for the electron beam centroid is

$$\ddot{u}(t) + i\Omega_0 \dot{u}(t) - \omega_0 \omega_w e^{i\omega_w t} u^*(t) + \sum_{i=1}^{M} \omega_i^2 f(|u - u_i|)(u(t) - u_i(t)) = 0, \qquad (21)$$

where $\omega_i^2 = 2N_i e^2/\gamma_0 m_0 r_b^2$, $M(t)$ is the total number of beamlets at time t, $u_i(t) = x_i(t) + iy_i(t)$ is the position of the ith ion beamlet, and $f(|u - u_i|) = 1$ for $|u - u_i| \leq r_b$, $(r_b/|u + u_i|)^2$ for $|u - u_i| > r_b$. Here, we have neglected the effect of the image fields of the wall, assuming that the quadrupole field is strong enough. Since the ions are continuously created the total number of beamlets, $M(t)$, increases linearly in time.

As is done previously we divide the drift motion of the beam centroid into the

drift center motion and the fast oscillatory motion of frequency ω_w, and average the motion over $2\pi/\omega_w$ in order to obtain the equation of motion for the drift center. The result is

$$\dot{u}_c(t) - i\omega'_B(t)u_c(t) - \frac{i}{\Omega_0}\sum_i \omega_i^2 f(d_i)(u_c(t) - u_i(t)) = 0, \tag{22}$$

where $\omega'_B(t) = \omega_0^2\omega_w^3(1 - \omega_w/\Omega_0)/[\omega_w^2(\Omega_0^2 - \omega_w^2) + \sum_i(\omega_i r_b/d_i(t))^4]$, and $d_i(t) = |u_c(t) - u_i(t)|$. Assuming that $\sum_i \omega_i^2 \ll \omega_w\Omega_0$, the bounce frequency is approximately constant; $\omega'_B(t) \approx \omega_B \approx (\omega_0/\Omega_0)^2\omega_w$.

In order to have a closed set of equations we need the equations for the ions. The ion beamlets move in the electrostatic field of the electron beam without seeing the external magnetic fields. The equation of motion, therefore, is

$$\ddot{u}_i(t) = -\frac{\omega_p^2}{2} f(d_i)[u_i(t) - u_c(t)], \tag{23}$$

where $\omega_p^2 = 4\pi n_e e^2/m_i$, and m_i is the ion mass. Here we are implicitly assuming that the ion density is much less than the beam electron density so that the ions do not see each other. Also the effect of image charges on the wall has been neglected.

To seek a numerical solution to (22) and (23), we normalize the variables; $\hat{t} = \omega_B t$ and $\hat{u}_{i,c} = u_{i,c}/r_b$. Rewriting the equations with these variables:

$$\hat{u}'_c(\hat{t}) - i\hat{u}_c(t) - i\eta\sum_i \delta\hat{t}_i f(d_i)(\hat{u}_c(\hat{t}) - \hat{u}_i(\hat{t})) = 0, \tag{24}$$

$$\hat{u}''_i(\hat{t}) + \mu f(d_i)[\hat{u}_i(\hat{t}) - \hat{u}_c(\hat{t})] = 0, \tag{25}$$

where $\eta = \omega_i^2/(\delta t_i\omega_B^2\Omega_0)$, $\mu = \omega_p^2/(2\omega_B^2)$, and primes denote derivatives with respect to $\hat{t}$. Notice that the parameter η is a measure of the strength of the drag force.

Now we solve (24) and (25) numerically. Figure 5 shows an example of the ion distribution in the minor cross section. Here, a circle indicates the position of the electron beam, and the ion beamlets are represented with following points. The electron beam rotates counterclockwise from its initial position $u_c(0) = 8r_b$. The ion beamlets are created during every tenth numerical time step and are placed at the electron beam center at the time of creation. Each beamlet is given with a charge density that is weighted by the time lapse since the last beamlet was created. The parameters in Figure 5 are $\eta = 2$ and $\mu = 5$. The figure shows the electron beam being tapped near the center in a single bounce period.

In Figure 6 we collect the decay rates of $|u_c(t)|$ varying the two independent parameters, μ and η. Here, the decay rates has been estimated with the amount of radius reduction after a single bounce time, i.e. $\Gamma = \ln(|u_c(2\pi)/u_c(0)|)/2\pi$, where $u_c(0) = 8r_b$ has been used. Strictly speaking, the decay rate is a function of time, i.e., the beam does not move toward the center according to a simple exponential law. As more and more ions are created, and as the beam bounce motion slows down, the trapping rate would be enhanced. Γ is, therefore, simply a measure of the decaying tendency. We notice that the decay rate in Figure 6 increases with increasing η and μ. The dependence on η is apparent. For a large η the ion density in each beamlet

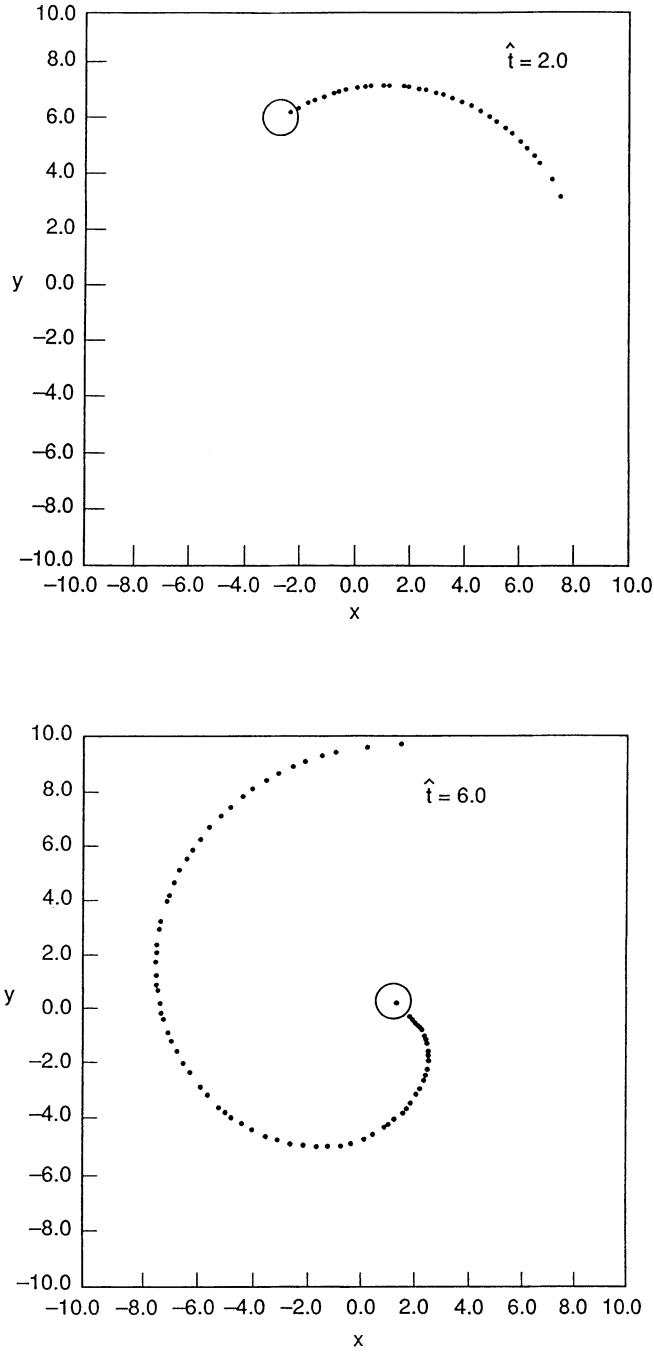

FIGURE 5 (a),(b) Ion distributions in a minor cross section for $\mu = 5$, $\eta = 2$. Electron beam (circle) was located initially at $x = 8$, $y = 0$, and subsequently moves counterclockwise. Ions (points) fall behind the beam, exerting a drag force. (b) shows the beam locating near the center in a bounce time $\hat{t} = \omega_B t$.

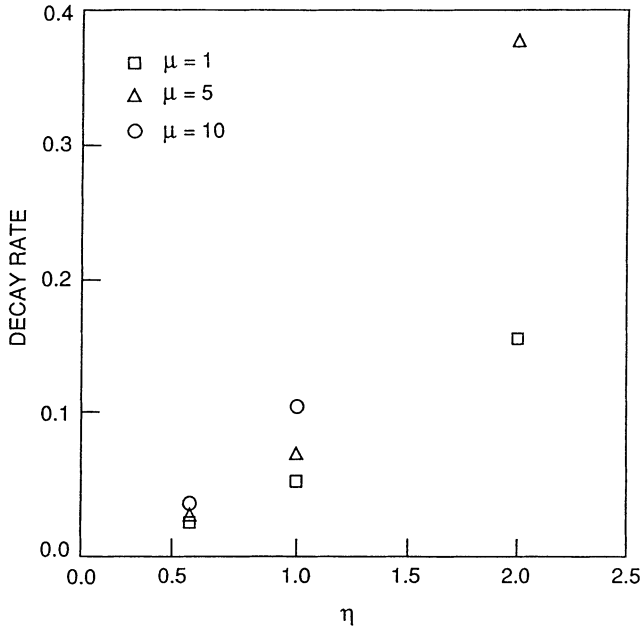

FIGURE 6 Decay rates in unit of ω_B for various values of parameters: □ $\mu = 1$, △ $\mu = 5$, ◇ $\mu = 10$.

is large, hence the electron beam feels a large drag force. The dependence on μ can be explained by considering how the ions are distributed. For large μ the ions feel a strong potential field, and as a result, ions are more closely attached to the electron beam, enhancing the drag force. If we further increase μ, however, the ions no longer fall behind the drifting electron beam; they catch up with the beam and locate themselves ahead of it. When this begins to happen, the decay rate drops. Figure 7 shows a situation like this. Here $\mu = 20$ has been chosen. Finally, we give a set of physical values which corresponds to $\mu = 10$ and $\eta = 1$; $\omega_B = 3 \times 10^7\ \text{sec}^{-1}$, $I_0 = 3$ kA, $B_0 = 2$ kG, $\gamma_0 = 2$, $r_b = 1$ cm, and vacuum pressure $\simeq 8 \times 10^{-5}$ torr.

5 ESTIMATION FOR THE NRL MODIFIED BETATRON

The present work has been performed as a part of the efforts to explain the beam trapping observed in the NRL modified betatron with a strong focusing field. In this section we estimate whether the trapping scheme suggested in the previous sections are relevant to the experimental observation. The physical parameters of the experiment are listed in Table 1.

In the experiment the electron beam is injected into the toroidal vacuum chamber from a diode placed inside the chamber. The diode is located 8 cm away from the minor axis. The applied voltage on the diode is 0.5 MV, which we may expect to be the initial beam energy. The beam temperature is presently unknown. The diode

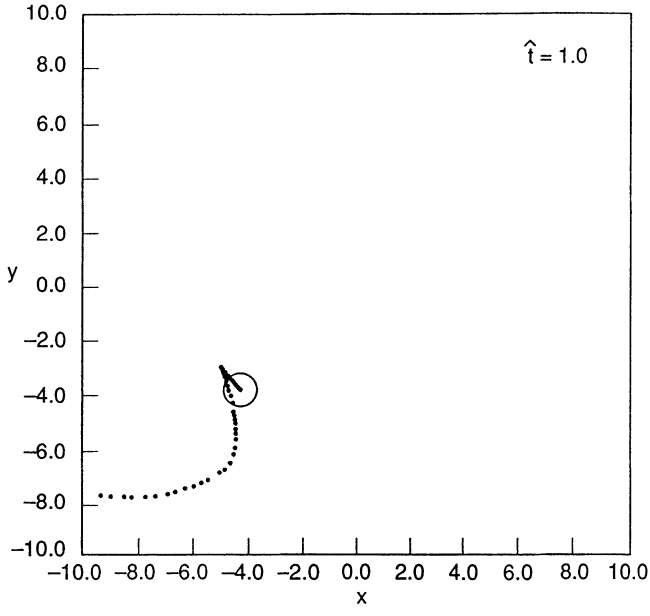

FIGURE 7 Ion distribution for $\mu = 20$, $\eta = 1$ at time $\hat{t} = 4$, showing that the ions oscillate around the electron beam due to a strong potential field. Ions ahead of the beam reduces the decay rate.

voltage pulse has a 20-ns rise time, a 40-ns flat top, and a 20-ns decay time. The electron ring current is mostly produced by the 40-ns flat-topped portion. Since the transit time around the torus is about 24-ns for an electron beam with an energy 0.5 MeV, it is expected that the electrons would form a two-turn ring initially. Each ring has a current of 700 A, and hence the total circulating current by the two turns is 1.4 kA. It seems, however, that only the first turn is being trapped. The trapped current is between 0.5–0.6 kA.

The drift motion of the injected beam in the minor cross section is monitored with a 10-μm-thick polycarbonate foil placed across a minor cross section. Light is emitted from the foil when the electrons pass through, and is recorded on an open-shuttered camera. The photographs show light spots spiraling in towards the minor axis of the vacuum chamber from the injection position. From the inter-spot distances we can infer that the bounce period is between 200–500 ns, which agrees well with the linear prediction in Section 2. For example, with a 16 kA current on the stellarator windings, the field gradient near the center is estimated to be $b_0 k_w \simeq 16$ G/cm, and hence, for a guiding field of 2 kG, the bounce frequency $\omega_B \simeq (\omega_0/\Omega_0)^2 \omega_w \simeq 2.9 \times 10^7\ \mathrm{s}^{-1}$, which gives a bounce period of $2\pi/\omega_B \simeq 220$ ns. The space-charge force, at this stellarator field, contributes little to the bounce frequency.

Usually, the beam approaches the center of the chamber within one or two bounce periods. This implies that the trapping rate is about the same as the inverse of the bounce period, $2\text{–}5 \times 10^6\ \mathrm{s}^{-1}$. For a beam current of a kiloampere we estimate the effect of image current displacement produces a trapping rate, from Equation

(10), of $\sim 10^5\ s^{-1}$. Since the wakefield enhances the rate by about a factor of two, we expect a decay time $\Gamma^{-1} \sim 5\ \mu s$, which differs from the observed value by an order of magnitude. Even though the calculations in Section 3 are valid in the linear regime, i.e., for a beam position near the minor axis, nonlinear corrections are expected not to exceed a few tens of percent. Hence, the resistive wall effect does not seem to be the major cause for the observed trapping.

The experiments were performed with a vacuum pressure between $2–8 \times 10^{-6}$ torr. If we assume that the electron beam is cold, and that the major ion source is the electron impact on the background gases, the pressure required to explain the observed trapping rate is about 10^{-4} torr. The ions, however, seem to help the beam trapping even though they do not have a major effect. It has been observed that the trapping behavior depends on the vacuum pressure. As the pressure is decreased the trapping becomes more difficult. In other words, the trapping requires stricter satisfaction of the equilibrium condition at lower pressure.

6 CONCLUSION

We have investigated dissipative beam trapping schemes in a modified betatron with strong focusing. As the sources for dissipation, the resistive wall and the background ions have been considered.

The resistive wall contributes to the beam trapping by introducing a radial magnetic field at the position of the beam. This magnetic field is produced by the image-current displacement and the wakefield. The former defines the time-asymptotic trapping behavior, and the latter defines the transient. For a current instantaneously turned on in a long cylindrical wall, the wakefield effect is shown to be minor. In a toroidal geometry, however, it is shown that the wakefield enhances the decay rate to more than twice the rate caused by the image current alone.

When the beam drift is fast enough, the heavy ions, which are produced by electron impact ionization, do not follow the beam. These ions are left behind the drifting beam, and exert a poloidal electric force to induce trapping. The relevant parameters for the interaction have been defined, and the behaviors of the beam and the ions have been shown through a simple numerical model.

Finally, an estimation has been made of the relevance of these schemes to the beam trapping observed in the NRL modified betatron. For the given experimental parameters we estimate that the trapping is not either from the resistive wall effect or from the electron impacted background gas ionization.

ACKNOWLEDGEMENT

The authors thank Dr. C. A. Kapetanakos and Dr. D. Dialetis for many helpful discussions. This work has been supported by the Office of Naval Research.

REFERENCES

1. C. A. Kapetanakos and P. Sprangle, Physics Today (February 1985).
2. H. Ishizuka et al., *Phys. Rev. Lett.* **53**, 266 (1984); J. Golden et al., in *Proceedings of the 7th International Conference on High-Power Particle Beams*, Vol. I, p. 221 (1988); V. Bailey et al., in *Proc. of the 1987 IEEE Part. Accel. Conf.*, p. 920; W. K. Tucker et al., *Proc. of 1987 IEEE Part. Accel. Conf.*, p. 957.
3. C. A. Kapetanakos and P. Sprangle, NRL Memo Report 5259, Naval Research Laboratory (Washington D.C., 1984).
4. P. Sprangle and C. A. Kapetanakos, *J. Appl. Phys.* **49**, 1 (1978); N. Rostoker, *Bull. Am. Phys. Soc.* **25**, 854 (1980); P. Sprangle, C. A. Kapetanakos, and S. J. Marsh, NRL Memorandum Report 4666 (1981); C. A. Kapetanakos, P. Sprangle, D. P. Chernin, S. J. Marsh, and I. Harper, *Phys. Fluids* **26**, 1634 (1983).
5. P. Sprangle and C. A. Kapetanakos, *Part. Accel.* **14**, 15 (1983).
6. C. W. Roberson, A. Mondelli, and D. Chernin, *Phys. Rev. Lett.* **50**, 507 (1983).
7. P. Sprangle and C. A. Kapetanakos, *Part. Accel.* **18**, 203 (1986).
8. A. W. Chao, *AIP* Conf. Proc. No. 105 (1982) p. 353.
9. The asymptotic expression is valid when $(16\pi\sigma a/c)^{1/3}(|z - ct|/a) \gg 1$. With $a = 15$(cm) and $\sigma = 3 \times 10^{14}$(/sec) the condition is translated to $|z - ct| \gg 1.2$ (mm).
10. F. F. Rieke and W. Prepejchal, *Phys. Rev.* A **6**, 1507 (1972).